International Journal of Neural Systems, Vol. 23, No. 3 (2013) 1350009 (15 pages)

DOI: 10.1142/S0129065713500093

World Scientific
www.worldscientific.com

AUTOMATED DIAGNOSIS OF EPILEPSY USING CWT, HOS AND TEXTURE PARAMETERS

U. RAJENDRA ACHARYA
Department of Electronics and Computer Engineering
Ngee Ann Polytechnic, Singapore 599489
Department of Biomedical Engineering, University of Malaya, Malaysia
aru@np.edu.sg

RATNA YANTI, ZHENG JIA WEI, M MUTHU RAMA KRISHNAN, TAN JEN HONG, ROSHAN JOY MARTIS and LIM CHOO MIN
Department of Electronics and Computer Engineering
Ngee Ann Polytechnic, Singapore 599489

Accepted 5 February 2013
Published Online 25 April 2013

Epilepsy is a chronic brain disorder which manifests as recurrent seizures. Electroencephalogram (EEG) signals are generally analyzed to study the characteristics of epileptic seizures. In this work, we propose a method for the automated classification of EEG signals into *normal*, *interictal* and *ictal* classes using Continuous Wavelet Transform (CWT), Higher Order Spectra (HOS) and textures. First the CWT plot was obtained for the EEG signals and then the HOS and texture features were extracted from these plots. Then the statistically significant features were fed to four classifiers namely Decision Tree (DT), K-Nearest Neighbor (KNN), Probabilistic Neural Network (PNN) and Support Vector Machine (SVM) to select the best classifier. We observed that the SVM classifier with Radial Basis Function (RBF) kernel function yielded the best results with an average accuracy of 96%, average sensitivity of 96.9% and average specificity of 97% for 23.6 s duration of EEG data. Our proposed technique can be used as an automatic seizure monitoring software. It can also assist the doctors to cross check the efficacy of their prescribed drugs.

Keywords: Electrocardiogram; higher order statistics; epilepsy; ictal; interictal; discrete wavelet transform; classifier.

1. Introduction

Epilepsy is a chronic neurological disorder characterized by recurrent unprovoked seizures.[1,2] These seizures are transient signs with symptoms of abnormal, excessive or synchronous neuronal activity in the brain.[3] Epilepsy affects nearly 3 million Americans and 50 million people worldwide.[4] In the US, it affects more than 300,000 children under the age of 15 — more than 90,000 of whom have seizures that cannot be adequately treated. The number of epilepsy cases in the elderly is climbing and more than 570,000 adults aging 65 and above have this condition.[4]

The characteristics of EEG signals depend on the mental state of the subject. These signals are highly complex, nonlinear and nonstationary in nature. It is very difficult to decipher the minute changes in the time scale manually due to small amplitude and random nature of the signal. Hence, there is a need to develop a computer-aided system to detect the normal, interictal and epilepsy classes. Nonlinear features extracted from the EEG signals may be helpful

to understand the working of billions of highly interconnected neurons in the brain. These nonlinear features may be able to unearth the hidden complexities existing in the EEG signals.[5]

Multi-stage nonlinear pre-processing filter in combination with an Artificial Neural Network was used for the automated detection of epilepsy.[6] Their proposed system was able to detect the epilepsy with an accuracy of 97.2%. Time and frequency domain features combined with Elam network was used for the automated detection of epilepsy.[7] Their proposed model was able to detect epilepsy with an accuracy of 99.6%.

Four entropies namely, Kolmogorov–Sinai entropy, approximate entropy, Shannon spectral entropy and Renyi's entropy coupled with Adaptive Neuro Fuzzy Inference System (ANFIS) were used for classification of epilepsy.[7] Their methods were able to detect seizure with an accuracy of more than 90%. Discrete Wavelet Transform (DWT) coefficients of normal and epileptic EEG signals[8–14] with Mixture of Experts (ME) were used to detect the two classes.[15] They obtained an accuracy of 94.5% which was higher than standalone neural net (93.2%).

Fast Fourier transform-based features coupled with decision tree (DT) classifier was able to classify the normal and epileptic EEG signals with accuracies of 98.68% and 98.72% using 5- and 10-fold cross-validation, respectively.[16] Approximate entropy features combined Elman and probabilistic neural networks yielded an overall classification accuracy of 100% to detect the normal and epileptic EEG signals.[17]

Various features of energy distribution in the time-frequency domain coupled with neural network were able to detect the epileptic EEG signals with an accuracy of more than 97.7%.[18] Approximate entropy (ApEn) values of the approximation and detail coefficients of DWT were computed.[19,20] ApEn values of the epileptic and the normal and epileptic EEG was able to detect with more than 96% accuracy. Without DWT pre-processing, it was able to detect up to 73%.

DWT coefficients of EEG signals were subjected to dimensionality reduction by principal component analysis (PCA), independent component analysis (ICA) and linear discriminant analysis (LDA) to classify into two classes: normal and epilepsy EEG signals.[21] Then these features with SVM classifier for automated detection of normal and epileptic EEG signal. Among the LDA method yielded 100% classification accuracy, sensitivity and specificity.

Normal, alcoholic and epileptic EEG signals were analyzed using nonlinear features namely Correlation Dimension (CD), Largest Lyapunov Exponent (LLE), Hurst exponent (H) and entropy.[22] They have proposed clinically significant unique ranges of nonlinear parameters for these classes ($p < 0.05$). Higher order spectra (HOS) technique was used to differentiate *normal*, *interictal* and *epileptic* EEG signals.[16,17] Unique ranges for HOS-based features were proposed for the different classes with high confidence level (p-value = 0.002). EEG signals were used as a diagnostic marker for Alzheimer's disease.[23–25]

In this work, we have proposed an automated, simple, fast and cost-effective efficient method to classify EEG signals to *normal*, *interictal* and *ictal* classes using Continuous Wavelet Transform (CWT), HOS, textures and classifiers. The proposed technique is illustrated by a block diagram in Fig. 1. Part of the dataset is used for building the classifier and

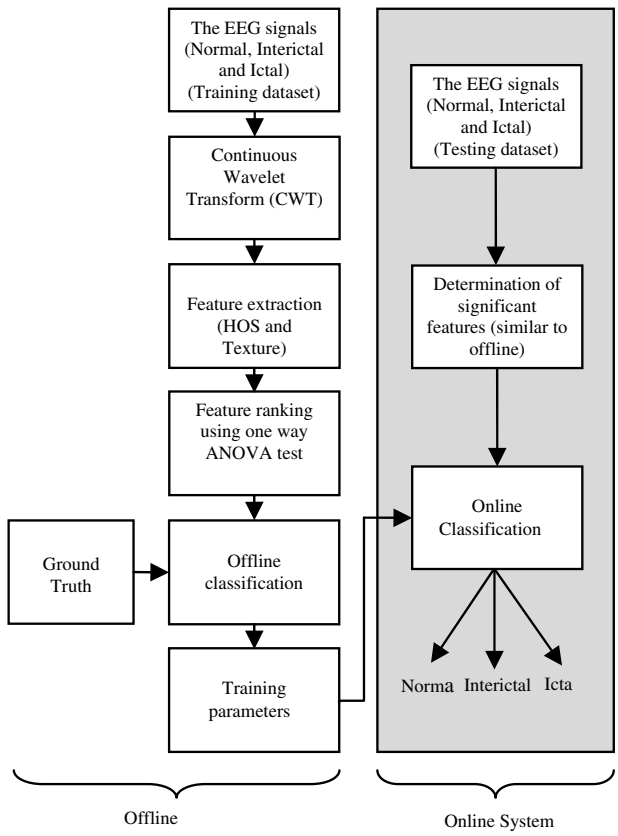

Fig. 1. Proposed system.

the rest is used for evaluating the classifier. First, we apply CWT to the EEG segments, and then we extract HOS and textures features from the resultant CWT image. Significant features are selected using the Analysis of Variance (ANOVA) test. These selected features and the Ground Truth (GT) of whether the segment is *normal*, *interictal* or *ictal* as determined by the physicians are used to train several classifiers to determine the optimum classifier parameters for real-time use. In the real-time online system, the features that were deemed significant by the offline system are extracted from the test segment whose class label is to be determined. The classifier parameters are applied on these features to determine the class label. The class labels of the test dataset that were predicted by the real-time system are used to determine performance measures such as accuracy, sensitivity and specificity.

The rest of the paper is structured as follows. The details of EEG data used in this work are given in Sec. 2. CWT of EEG data, HOS and texture features are discussed in Sec. 3. Various classifiers used in this work are briefly described in Sec. 4. Results of the work are presented in Sec. 5 and discussed in Sec. 6. Finally, the paper concludes in Sec. 7.

2. EEG Data

In this work, we have used artifact free EEG signals taken from the EEG time series data available at the Department of Epileptology, University of Bonn.[26] 100 segments of EEG signals were taken from five healthy subjects and 100 segments of data in each of the *interictal* and *ictal* epileptic classes were obtained from five epileptic patients. Normal EEG signals were taken from standard surface electrode placement scheme (the international 10–20 system). Epileptic EEG signals were collected from intracranial electrodes of the correct epileptogenic zone.[27–33] The *interictal* segments contained only activity recorded during seizure free intervals. During the *ictal* category, signals were selected from the *ictal* activity recording sites. These EEG signals were recorded using a 128-channel amplifier system, digitized with a sampling rate of 173.61 Hz and 12-bit A/D resolution, and filtered using a 0.53∼40 Hz (12 dB/octave) band pass filter. Typical *normal*, *interictal* and epileptic (*ictal*) EEG signals are shown in Fig. 2.

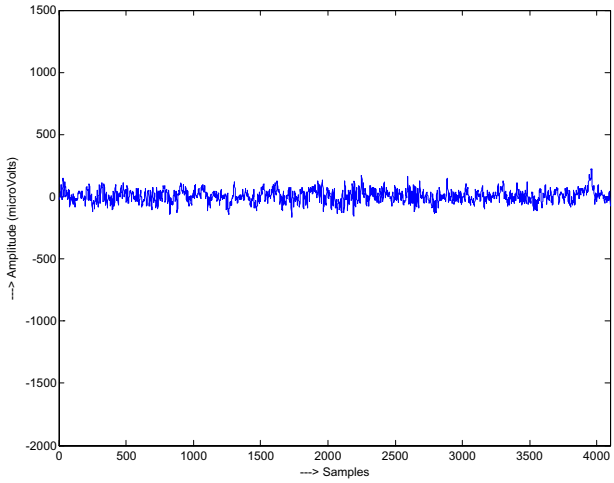

(a)

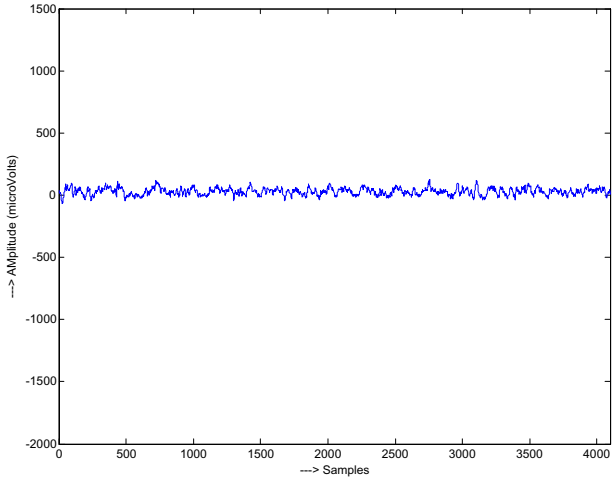

(b)

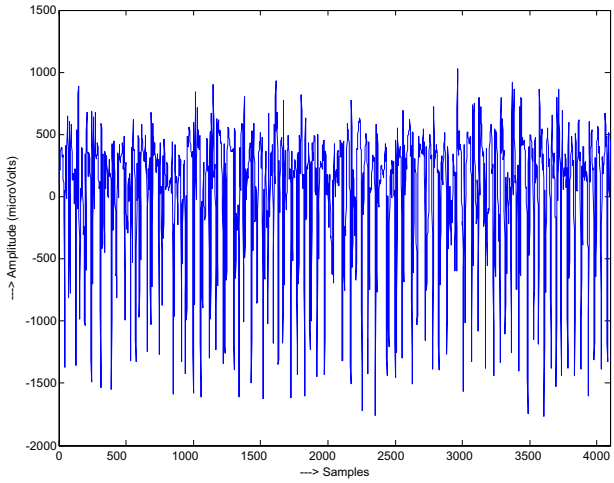

(c)

Fig. 2. Typical EEG signals: (a) normal, (b) interictal and (c) ictal.

3. Methodology

In this work, we have first obtained the scalogram of the EEG signal using CWT. Then the HOS and texture features were extracted from the scalogram images. ANOVA test was used to select the clinically significant features ($p < 0.05$). Then these features were fed as input to the classifiers for automated classification. We have briefly explained the CWT, HOS and texture methods in the following sections.

3.1. *Continuous wavelet transform (CWT)*

Wavelet is a small wave of finite duration.[34–44] Wavelet analysis essentially involves comparing the signal with a chosen (finite duration) *wavelet*; and recording the correlation coefficient.[45,46] Wavelet analysis is of two types: Continuous time Wavelet Transform (CWT) and Discrete Wavelet Transform (DWT).[47]

In this work, we have used CWT for our analysis. By dilating (scaling) the *wavelet* in the time axis to different durations coefficients are evaluated and this process is repeated. This will yield a 3D scalogram plot with X-axis depicting the translation of the wavelet, dilation in Y-axis, and value of coefficients indicated as pixel value in the Z-axis. There are many standard wavelet functions (*mother wavelets*) available in MATLAB toolbox and are selected based on the application. In this work, we have used *Mexican hat* mother wavelet function.[48] Figures 3(a)–3(c) show the typical scalogram plot of *normal*, *interictal* and *ictal* EEG signals, respectively (corresponding to Fig. 2 EEG signals).

3.2. *Higher order spectra (HOS)*

It is a nonlinear method which can be used to extract the subtle changes in the signal. It is more robust to noise and performs well for even noisy physiological signals.[27] It is able to reveal deviation of Gaussianity and phase information of the signal. HOS can be used for both deterministic signals and random processes.[13] We derived the features from the third-order statistics of the signal, namely, the bispectrum and is given by

$$B(f_1, f_2) = E[X(f_1)X(f_2)X*(f_1 + f_2)], \quad (1)$$

where $X(f)$ is the Fourier transform of the signal $x(nT)$ and $E[\cdot]$ stands for the expectation operation.

Features are calculated by integrating the bispectrum along the dashed line with slope $= a$. Frequencies are normalized by the Nyquist frequency (Fig. 4). These bispectral invariants[49] contain information about the shape of the waveform within the

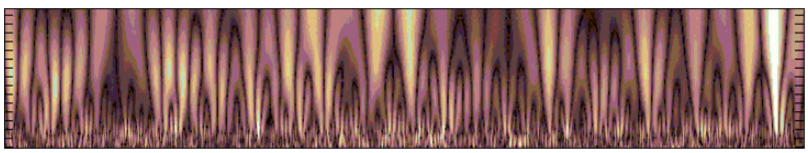

(a)

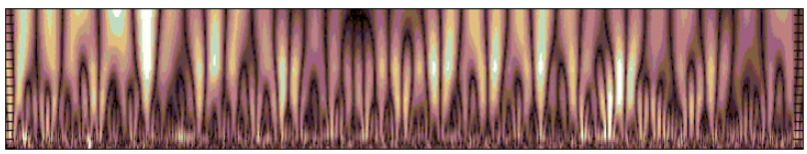

(b)

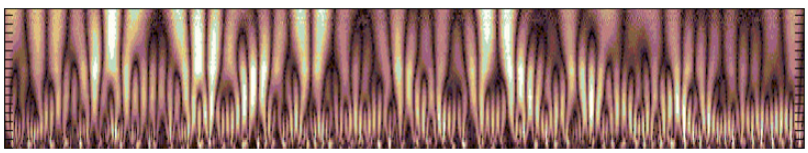

(c)

Fig. 3. Typical CWT plots: (a) normal, (b) interictal and (c) ictal.

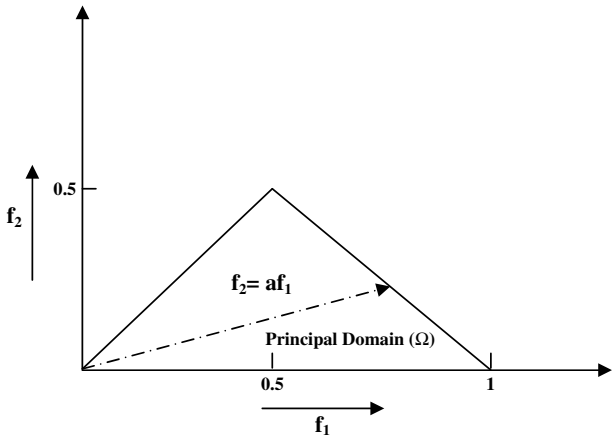

Fig. 4. Nonredundant region (Ω) of computation of the bispectrum for real signals.

window and are invariant to shift and amplification and robust to time-scale changes. In this work, we evaluated five HOS features for every 10^0. Bispectral entropies derived from bispectrum have been used to detect the cardiac arrhythmia and epilepsy.[27,50,51] The equations of the various HOS features are given below:

Mean of Magnitude:

$$M_{\text{ave}} = \frac{1}{L}\sum_{\Omega} |B(f_1, f_2)|. \tag{2}$$

Phase Entropy:

$$P_e = \sum_n p(y_n) \log p(y_n). \tag{3}$$

Normalized Bispectral Entropy (BE 1):

$$\text{Ent1} = -\sum_n p_n \log p_n, \tag{4}$$

where $p_n = \frac{|B(f_1,f_2)|}{\sum_\Omega |B(f_1,f_2)|}$, and Ω is the region as shown in Fig. 4.

Normalized Bispectral Squared Entropy (BE 2):

$$\text{Ent2} = -\sum_n q_n \log q_n, \quad \text{where}$$
$$q_n = \frac{|B(f_1, f_2)|^2}{\sum_\Omega |B(f_1, f_2)|^2}. \tag{5}$$

Normalized Bispectral Cubic Entropy (BE 3):

$$\text{Ent3} = -\sum_n r_n \log r_n, \quad \text{where}$$
$$r_n = \frac{|B(f_1, f_2)|^3}{\sum_\Omega |B(f_1, f_2)|^3}. \tag{6}$$

The H parameters are related to the moments of bispectrum. The sum of logarithmic amplitudes of the bispectrum:

$$H_1 = \sum_{f_1, f_2 \in \Omega} \log(|B(f_1, f_2)|), \tag{7}$$

where $B(f_1, f_2)$ is the bispectral content of the signal at the point (f_1, f_2) in the Ω region.

The sum of logarithmic amplitudes of diagonal elements in the bispectrum:

$$H_2 = \sum_{f_k \in \Omega} \log(|B(f_k, f_k)|), \tag{8}$$

where $B(f_k, f_k)$ is the bispectral content of the signal at the diagonal elements (f_k, f_k) in the Ω region.

The first-order spectral moment of the amplitudes of diagonal elements in the bispectrum:

$$H_3 = \sum_{k=1}^{N} k \log(|B(f_k, f_k)|), \tag{9}$$

where N is the number of diagonal elements in the bispectrum plot in the Ω region.

The second-order spectral moment of the amplitudes of diagonal elements in the bispectrum:

$$H_4 = \sum_{k=1}^{N} (k - H_3)^2 \log(|B(f_k, f_k)|), \tag{10}$$

where N is the number of diagonal elements in the bispectrum plot in the Ω region and H_3 represents the first-order spectral moment of the amplitudes of diagonal elements.

$$H_5 = \sum_{k=1}^{N} (k - H_4)^2 \log(|B(f_k, f_k)|). \tag{11}$$

All the above features are again defined over the principal domain Ω in Fig. 4.

3.3. *Texture features*

Texture features indicate the properties like smoothness, coarseness and regularity, among intensity values of neighboring pixels.[52] Such features can be used as features for the automated classification. In this work, we have extracted the texture features derived from gray level co-occurrence matrix (GLCM) and run-length matrix. A brief explanation of them is

given below:

3.3.1. *Co-occurrence matrix*

For an image of $M \times N$, the GLCM is defined[53] as

$$C_d(i,j) = \left| \left\{ \begin{array}{l} (p,q),(p+\Delta x, q+\Delta y): \\ \quad I(p,q) = i, I(p+\Delta x, q+\Delta y) = j \end{array} \right\} \right|, \tag{12}$$

where (p,q), $(p+\Delta x, q+\Delta y) \in M \times N$, $d = (\Delta x, \Delta y)$ and $|\cdot|$ denotes the cardinality of a set. Given a gray level i in an image, the probability that a pixel at a $(\Delta x, \Delta y)$ distance away is j is:

$$P_d(i,j) = \frac{C_d(i,j)}{\sum C_d(i,j)}. \tag{13}$$

Correlation:

$$\text{Corr} = \sum_i \sum_j [(ij) P_d(m,n)] - \mu_i \mu_j \Big/ \sigma_i \sigma_j, \tag{14}$$

where

$$\mu_i = \sum i P_d(i,j), \quad \sigma_i^2 = \sum i^2 P_d(i,j) - \mu_i^2, \tag{15}$$

$$\mu_j = \sum j P_d(i,j), \quad \sigma_j^2 = \sum j^2 P_d(i,j) - \mu_j^2. \tag{16}$$

3.3.2. *Run length matrix*

Higher order statistical features are extracted from run length matrix. Run length matrix $P_\theta(i,j)$ records the frequency that j points with a gray level i continue in the direction θ. The ith dimension of the matrix corresponds to the gray level and has a length equal to the maximum gray level, n, while (j)th corresponds to the run length and has length equal to the maximum run length, l. We have used the texture measure from run length matrix of $\theta = 0^\circ$ computed by Refs. 54 and 55 and is given below.

Short run emphasis (SRE):

$$\sum_i \sum_j \frac{P_\theta(i,j)}{j^2} \Big/ \sum_i \sum_j P_\theta(i,j). \tag{17}$$

3.3.3. *Local binary pattern*

The local binary pattern (LBP) is a simple and fast method for multi-scale local texture analysis.[56,57] The spatial structure information is combined with contrast which is a measure of the amount of local texture. In this work, we have extracted the LBP features on CWT images of *normal*, *interictal* and *ictal* classes. In order to evaluate LBP, a circular neighborhood around a pixel with P points on the circumference of the circle with radius R such that they are all equidistant from the center pixel is chosen. Figure 5 shows circularly symmetric neighbor sets for different values of P and R.

Let g_c be the center pixel gray value and g_p, $p = 0, \ldots, P-1$, be the gray values of P number of pixels around g_c. If the value of $g_p > g_c$ then g_p will be 1 else it will be 0. Hence, P points will be converted to bitstream of 0s and 1s in a circular pattern.

$$\text{LBP}_{P,R}^{\text{rin2}} = \begin{cases} \displaystyle\sum_{p=0}^{P-1} s(g_p - g_c) & \text{if } U(\text{LBP}_{P,R}) \le 2 \\ P+1 & \text{otherwise.} \end{cases} \tag{18}$$

Then the binary bits are arranged in an array $T(g_0, g_1, \ldots, g_{p-1})$. The ASCII value of this value is assigned to g_c.

$$\mu = \frac{1}{P} \sum_{p=0}^{P-1} g_p, \tag{19}$$

$$\text{VAR}_{P,R} = \frac{1}{P} \sum_{p=0}^{P-1} (g_p - \mu)^2. \tag{20}$$

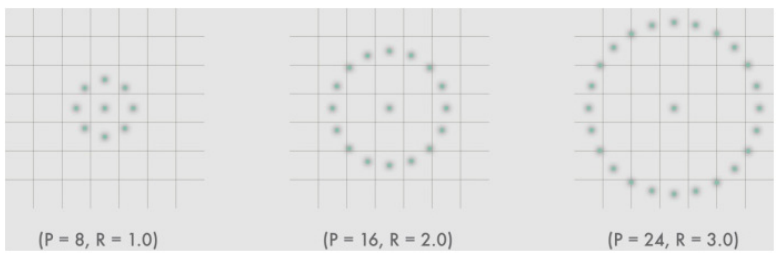

Fig. 5. Circularly symmetric neighbor sets for different P and R.

3.3.4. *Laws mask energy (LME)*

Various textures can be differentiated using the several masks of appropriate sizes.[58,59] It involves the application of such masks to the image and then evaluating the energy within the pass region of filters.[58] Three one-dimensional (1D) vectors L3 = [1 2 1], E3 = [−1, 0, 1] and S3 = [−1, 2, −1] are used to estimate the texture energies corresponding to the features namely: level, edge and spot, respectively. Nine two-dimensional (2D) masks of size 3 × 3, namely, L3L3, L3E3, L3S3, E3E3, E3L3, E3S3, S3S3, S3L3 and S3E3 are generated by convolving 1D horizontal vector with vertical 1D vector.

Except L3L3, all the other masks have zero mean. In this work, we have used these eight zero-sum masks numbered 1 to 8. In order to extract the texture information from an image $I(i, j)$, first the image has to be convoluted with each 2D mask. If we used L3S3 to filter the image $I(i, j)$, the resulting texture image will be

$$\mathrm{TI}_{\mathrm{L3S3}} = I(i, j) \otimes \mathrm{L3S3}. \tag{21}$$

In order to make the resultant images contrast independent, the texture image $\mathrm{TI}_{\mathrm{L3L3}}$ was used to normalize the contrast of all other texture images as shown in the following equation[58,59]:

$$\mathrm{Normalize}(\mathrm{TI}_{\mathrm{mask}}) = \frac{\mathrm{TI}_{(i,j)^{\mathrm{mask}}}}{\mathrm{TI}_{(i,j)^{\mathrm{L3L3}}}}. \tag{22}$$

Then the Texture Energy Measurements (TEM) are evaluated using the following equation[58,59]:

$$\mathrm{TEM}(i, j) = \sum_{u=-3}^{3} \sum_{v=-3}^{3} |\mathrm{TI}_{(i+u,j+v)}|. \tag{23}$$

Eight features using eight masks were extracted, denoted by LME1, LME2, etc. A more detailed analysis of applications of Law's texture can be found in the recent book by Mirmehdi *et al.*[52]

4. Classification

In this work, we have used four classifiers namely Decision Tree (DT), K-Nearest Neighbors (*KNN*), Probabilistic Neural Network (*PNN*) and Support Vector Machine (*SVM*). A brief description of the classifiers is given below.

4.1. *Various classifiers*

4.1.1. *DT classifier*

This classifier helps to make the analysis simpler by splitting the complex-decision processes into simpler decisions.[60] Tree like structure is generated in the output at the end of the classification. Training data set is partitioned in a recursive way until each partition consists of dominant samples from each class. The rules derived from tree are used to identify the unknown class.

4.1.2. *K-nearest neighbor (KNN)*

KNN classifier is an instance-based classifier where the unknown sample classified according to some distance or similarity criteria.[61] It is the simplest classification algorithm and the test data is classified by a majority vote of its neighbors. The unknown data is classified to a class which is most common among its K (small positive number) nearest neighbors. The contribution of the nearest samples is more than the farthest samples. In this work, we have chosen $K = 2$.

4.1.3. *Probabilistic neural network (PNN)*

PNN is a multi-layered feed forward network which consists of four layers: Input layer, Pattern layer, Summation layer and output layer. The advantages of PNN classifier are: trains faster, parallel structure, guaranteed to converge to an optimal classifier if the number of training set increases and training samples can be added or removed without extensive retraining.[62–64] The smoothing parameter (σ) controls the scale factor of the exponential activation function need to be chosen correctly to get the highest classification accuracy. In this work, we have obtained the highest performance using $\sigma = 0.284$.

4.1.4. *Support vector machine (SVM)*

SVM maps samples to points in a space in such a way that samples belonging to separate categories (i.e. classes) are divided or separated by a very clear gap that is as wide as possible.[65] When the new test data are applied, they will be mapped to the same space. The decision on the class of test data is made based on which side of the gap the data maps. Hyperplane is used to classify two classes and

a set of hyperplanes are used to classify multiclass problem. The best hyperplane yields the largest separation gap between the two classes. SVM classifier transforms nonlinear data to a separable form with the help of various kernel functions. In this work, we have used polynomial kernel of order one, and Radial Basis Function (RBF) kernel. The performance of SVM classifier depends on cost function (C) and width (σ) of the Gaussian kernel. In our work, we achieved highest classification accuracy using $C = 100$ and $\sigma = 0.001$.

4.2. *Classification process and performance evaluation*

All the classifiers were trained and tested using 10-fold cross-validation technique. A total of 300 datasets were used for training and testing with 100 datasets from each of the three classes, *normal*, *interictal* and *ictal*. These 300 samples were sub-divided into 10 equal parts (roughly). During each fold, 270 datasets were used for training and 30 data sets were used for testing. This process is repeated for nine more times. The overall performance of the classifier is evaluated by taking the average of 10 folds. In this work, we have evaluated the sensitivity, specificity, Positive Predictive Value (PPV) and accuracy. They are briefly explained below:

TN (True Negative) = Number of *normal* data classified as *normal*.
FN (False Negative) = Number of *ictal* and *interictal* data classified as *normal*.
TP (True Positive) = Number of *ictal* and *interictal* data correctly classified as they are.
FP (False Positive) = Number of *normal* data classified as abnormal (*ictal or interictal*).
Sensitivity = TP/(TP + FN).
Specificity = TN/(TN + FP).
PPV = TP/(TP + FP).
Accuracy = (TP + TN)/(TP + FN + TN + FP).

5. Results

The proposed methodology was implemented using the EEG signal of three classes. The scalogram of wavelet coefficients using Mexican hat wavelet is shown plotted in Figs. 3(a) to 3(c) for sample *normal*, *interictal* and *ictal* EEG waveforms. Several features extracted from the scalogram are listed in Table 1. It can be seen from the table that the features are clinically significant ($p < 0.05$).

Mean bispectrum magnitude (mAmp) and moments of bispectrum (H5) show higher values

Table 1. Range (Mean ± Standard Deviation) of features extracted from normal, interictal and ictal EEG signals.

Features	Normal	Interictal	Ictal	P-value
		HOS		
mAmp (0°)	8.61E + 13 ± 1.5E + 13	9.69E + 13 ± 2.57E + 13	7.34E + 13 ± 2.08E + 13	< 0.0001
H5 (0°)	8.65E + 18 ± 1.4E + 18	9.62E + 18 ± 1.61E + 18	7.83E + 18 ± 2.05E + 18	< 0.0001
ent1 (30°)	0.3445 ± 0.0471	0.3495 ± 0.047	0.3864 ± 0.0536	< 0.0001
ent2 (120°)	0.0533 ± 0.0381	0.0413 ± 0.0242	0.0785 ± 0.0493	< 0.0001
ent3 (120°)	0.0184 ± 0.0282	0.0095 ± 0.01	0.0377 ± 0.0395	< 0.0001
		Texture		
Correlation	0.851 ± 0.0121	0.8622 ± 0.024	0.826 ± 0.0238	< 0.0001
Short Run Emp	0.9743 ± 0.0029	0.9723 ± 0.0052	0.9773 ± 0.0053	< 0.0001
LME 1	3.01 + 09 ± 2.92E + 08	3.05 + 09 ± 4.23E + 08	3.42 + 09 ± 5.44E + 08	< 0.0001
LME 2	2.45 + 09 ± 2.45E + 08	2.36 + 09 ± 3.33E + 08	3.17 + 09 ± 5.31E + 08	< 0.0001
LME 4	32055962 ± 2793565	25332027 ± 3134957	39477884 ± 10883619	< 0.0001
LME 7	22291597 ± 3116183	17599834 ± 2878645	27177359 ± 8930424	< 0.0001
LME 8	26639488 ± 3827407	19514473 ± 3247197	33452436 ± 13537931	< 0.0001
LBP 2	0.1895 ± 0.008	0.1737 ± 0.0056	0.2019 ± 0.0236	< 0.0001
LBP 3	0.3186 ± 0.0082	0.3066 ± 0.0062	0.3254 ± 0.0178	< 0.0001
LBP 8	0.4611 ± 0.0141	0.4454 ± 0.0151	0.4928 ± 0.037	< 0.0001

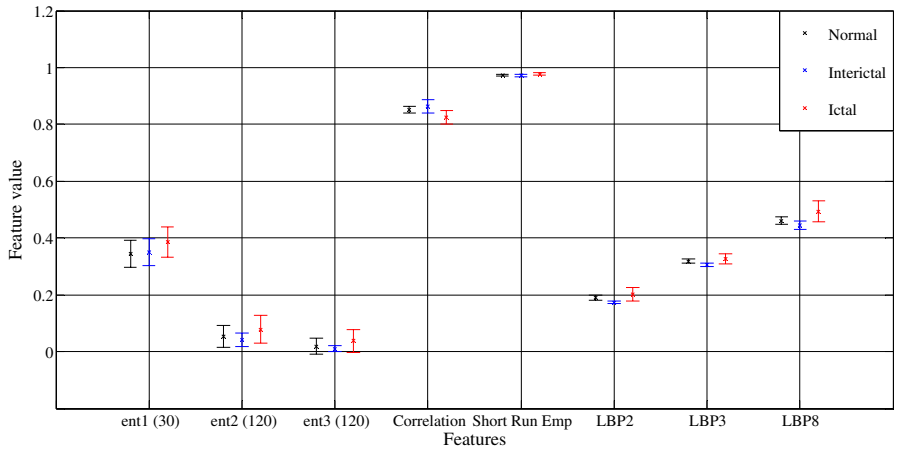

Fig. 6. Box plot of the range (the mean and standard deviation) of different features used.

for *interictal* as compared to the *ictal* and *normal* classes. Bispectrum entropies (ent1 (30°), ent2 (120°) and ent3 (120°)), Laws mask energies (LME1, LME2, LME4, LME7, LME8) and local binary patterns (LBP2, LBP3, LBP8) are showing higher value for *ictal* class due to higher variation (more disorder) as compared to the *interictal* and *normal* class (See Fig. 2). Due to the lower variation, correlation is higher (0.8622 ± 0.024) for *interictal* class as compared to the *normal* and *ictal* class. The ranges of different features (the mean and standard deviation) were shown graphically in Fig. 6.

The sensitivity, specificity, PPV, accuracy with the respective True Positives (TP), False Negatives (FN), True Negatives (TN) and False Positives (FP) for each of the classifiers used is tabulated in Table 2. It was observed that SVM with RBF kernel provided highest performance with 96% of accuracy, 96.9% of sensitivity, 97% of specificity and 98.5% of PPV, respectively.

Table 3 shows the classification accuracy of different feature combinations. It can be shown from the table that HOS features alone provided an average accuracy of 58.7%, average sensitivity of 84% and specificity of 30%. We have obtained average accuracy of 91%, average sensitivity of 95.1% and specificity of 94% using textures alone. The combination of HOS and texture features has provided an average

Table 2. The sensitivity, specificity, accuracy and PPV values presented by the six classifiers using all six features for training and testing (Mean ± Standard Deviation).

Classifiers	TN	FN	TP	FP	Accuracy	PPV	Sensitivity	Specificity
DT	8	2	18	2	84	89.8	90	79
PNN	9	2	18	2	86.7	92.5	90.5	85
KNN	8	2	18	2	84.7	91.1	88.5	82
SVM (rbf)	**10**	**1**	**19**	**0**	**96**	**98.5**	**96.9**	**97**
SVM (poly1)	9	1	18	1	90.7	95	93.3	90

Table 3. The sensitivity, specificity, accuracy and positive predictive value registered by the SVM classifier for various feature combinations (Mean ± Standard Deviation).

Feature set	TN	FN	TP	FP	Accuracy	PPV	Sensitivity	Specificity
HOS	3	3	15	7	58.7	67.3	84	30
Texture	9	1	18	1	91	97	95.1	94
All features (HOS + Texture)	10	1	19	0	96	98.5	96.9	97

accuracy of 96%, average sensitivity of 96.9% and specificity of 97%.

6. Discussion

It can be seen from Table 1 that, entropies, LBP features and LMEs are having higher values for the *ictal* state than *interictal* state. During the *interictal* state, epileptic neurons at the epileptic zone will be isolated due to the reduced connections.[66] With the reduced connection the neurons may become idle and result in sudden increase in neural discharge causing an epileptic seizure. As a result, variability and entropy increases. During this state (seizure), the number of neurons available for processing the useful information reduces.[67,68] Table 4 summarizes the studies conducted for the automated identification of *normal*, *interictal* and *ictal* classes using the same database. Three EEG classes were classified using wavelet analysis and spiking neural network (SNN).[69] SpikeProp, Quick-Prop and RProp training algorithms were used to train SNN. RProp model yielded the maximum classification accuracy of 92.5%. The same group automatically classified the three classes using wavelet analysis, back propagation neural network and mixed-band feature space consisting of nine parameters.[70] Their proposed system was able to classify with an accuracy of 96.7% correctly.

PCA was applied to the nine-parameter mixed-band feature space and obtained an accuracy of 96.6% using a cosine radial basis function neural network (RBFNN) in classifying the three EEG classes.[71] They classified the three classes using the mixed-band feature space, obtained an accuracy of 90.7% to 94.8% for the three-class identification a multi-spiking neural network is used where information transfer between neurons is through synapses.[72]

Recently, Martis *et al.* automatically classified EEG of normal, interictal and ictal subjects using a novel nonlinear method called Empirical Mode Decomposition (EMD) and DT classifier.[73] They have reported a highest average accuracy of 95.33%, average sensitivity of 98% and average specificity of 97% using C4.5 DT classifier.

Table 4. Summary of studies that present various approaches to epilepsy detection using features extracted from EEG signals from the same dataset used in this study.

Authors	1. Features (No. of features)	Classifier	Accuracy(%)
Faust *et al.*[74]	Frequency domain parameters (8)	ANN, SVM and GMM	93.3
Ghosh-Dastidar *et al.*[70]	Mixed-band feature space (9)	Back Propagation Neural Network	96.7
Ghosh-Dastidar and Adeli[69]	Mixed-band feature space (9)	Spiking Neural Network	92.5
Ghosh-Dastidar *et al.*[72]	Mixed-band feature space (9)	Multi-Spiking Neural Network	90.7–94.8
Martis *et al.* (2012)[73]	EMD features	C4.5 DT classifier	95.3
Ghosh-Dastidar *et al.*(2008)[71]	Mixed-band feature space (9)	Radial Basis Function Neural Network	96.6
Guler *et al.*[75]	Lyapunov exponents (4)	Recurrent Neural Network	96.79
Chua *et al.*[51,74]	HOS-based features (3)	SVM and GMM	93.11
Acharya *et al.*[76]	Nonlinear features (5)	SVM and GMM	95
Acharya *et al.*[77]	RQA parameters (10)	SVM	95.6
Acharya *et al.*[78]	Entropies (4)	Fuzzy	98.1
Acharya *et al.*[79]	Wavelet packet decomposition (WPD) and HOS cumulants (4)	Fuzzy	98.5
Acharya *et al.*[80]	PCA eigenvalues from WPD coefficient s(9)	GMM	99
Acharya *et al.*[28]	Entropies + HOS + Higuchi FD + Hurst (6)	Fuzzy	99.7
Acharya *et al.*[81]	DWT, ICA coefficients (10)	SVM	96
Martis *et al.*[73]	Intrinsic Mode Functions (7)	C4.5	95.33
This work	CWT, HOS and textures (15)	SVM	96

Lyapunov exponents coupled with recurrent neural network (RNN) classifier delivered a classification accuracy of more than 96%.[75] The Levenberg–Marquardt algorithm was used to train the RNN classifier to overcome the problem of slow convergence and yielded a good cost function compared with the other training algorithms.

Five nonlinear features namely correlation dimension, largest Lyapunov exponent, fractal dimension, Hurst exponent and approximate entropy coupled with GMM (Gaussian Mixture Model) classifier was able to classify three classes with an accuracy of 95%, sensitivity of 92.22% and specificity of 100%.[76]

HOS features namely, bispectrum invariants, and two normalized phase entropies coupled with GMM was able to automatically identify the three classes with a classification accuracy of 93.11%, sensitivity and specificity of 97.6% and 92%, respectively.[74] Same three features extracted from HOS and power spectrum were used to classify the three classes.[51] Their results show that the selected HOS-based features yielded 93.11% classification accuracy and 88.78% with features derived from the power spectrum for a GMM classifier.

Three peak amplitudes and their corresponding three frequencies in the frequency domain combined with SVM classifier presented an accuracy of 93.33%, sensitivity of 98.33% and specificity of 96.67%, respectively in classifying the three classes.[80]

EEG signals were decomposed into wavelet coefficients using WPD, and extracted eigenvalues from the resultant wavelet coefficients using PCA.[82] Significant eigenvalues, selected using the ANOVA test, were used to train and test several supervised classifiers using the 10-fold stratified cross-validation technique. They obtained classification accuracy, sensitivity and specificity of 99% using the GMM classifier.

Nonlinear features based on the HOS, two entropies, namely the Approximation Entropy (*ApEn*) and the Sample Entropy (*SampEn*), fractal dimension and Hurst exponent were extracted from the EEG signals.[28] Selected six features with the Fuzzy classifier resulted in 99.7% classification accuracy, sensitivity and specificity of 100%.

Four entropy features namely *ApEn*, *SampEn*, Phase Entropy 1 ($S1$) and Phase Entropy 2 ($S2$) were extracted from the *normal*, *interictal* and *ictal* EEG signals.[78] These features were fed to seven different classifiers: Fuzzy Sugeno Classifier (FSC), Support Vector Machine (SVM), K-Nearest Neighbour (KNN), Probabilistic Neural Network (PNN), Decision Tree (DT), Gaussian Mixture Model (GMM) and Naive Bayes Classifier (NBC). Our results show that the Fuzzy classifier was able to differentiate the three classes with a high accuracy of 98.1%.

Four clinically significant (p-value < 0.0001) HOS-based cumulant measures were extracted after the WPD.[79] Then these four cumulant features were fed to the several classifiers. It was observed that the Fuzzy classifier presented a high detection accuracy of 98.5%, sensitivity and specificity of 100% thereby establishing the possibility of effective epileptic activity detection using the proposed technique.

Ten Recurrence Quantification Analysis (RQA) parameters were used to quantify the important features in the EEG signals.[77] These features were fed to seven different classifiers: Support vector machine (SVM), Gaussian Mixture Model (GMM), Fuzzy Sugeno Classifier, K-Nearest Neighbor (KNN), Naive Bayes Classifier (NBC), Decision Tree (DT) and Radial Basis Probabilistic Neural Network (RBPNN) to select the best classifier. Their results show that the SVM classifier was able to identify the EEG classes with an average efficiency of 95.6%, sensitivity and specificity of 98.9% and 97.9%, respectively. Same group have classified the three classes by applying ICA on the DWT coefficients for various duration of EEG signals (6 s, 12 s, 18 s and 23.6 s).[81] They have obtained highest classification accuracy of 96%, sensitivity of 96% and specificity of 97% using SVM classifier for 23.6 s interval data.

In this work, we have obtained an average classification accuracy of 96%, average sensitivity of 96.9% and average specificity of 97%. Thus, the performance of CWT, HOS and texture combination is comparable to that obtained using nonlinear features. The novelty of this work is the application of textures, HOS and CWT for the detection of epileptic EEG signals. Also, we have proposed unique CWT plots for the three classes. The texture measures LBP, LME and HOS entropies capture the subtle variations in the EEG signals successfully.

The subtle changes in the EEG signals during *normal*, *interictal* and *ictal* state are not well captured in the time domain and frequency domains. The minute variations are manifested clearly as gray

level variations in the CWT image. The images follow some unique pattern of pixel intensities. They are self-similar and repeat in the time–frequency coordinates. This variation of pixel intensities is termed as texture. The CWT provides a few coefficients characterizing the texture of these images over time–frequency. Different texture descriptors are used to enhance the certain variations in the gray levels. During *ictal* state, due to the sudden neuronal firing there will be sudden change in the time–frequency domain resulting in the proportional change in the pixel intensity levels. In effect, the texture of the *interictal* and *ictal* images will be different than normal.

HOS also provides texture whose quantification is slightly different from the CWT. The HOS provides deviations from Gaussianity and the nonlinearity associated with these images. HOS provides the difference which was not felt with the first two order statistics methods like CWT. So effectively the method explores and demonstrates how the combination of two different texture measures can be used in classification of normal and abnormal patterns with a good accuracy.

The classification accuracy can be further increased by using other texture measures and time–frequency representations like Wigner Ville distribution, Hilbert Huang transform (HHT), Page distribution, Choi–William distribution, etc. The authors propose to do this study in their subsequent works.

7. Conclusion

The EEG signals are noise-like and complex in nature. It is very difficult to diagnose the brain related abnormalities using these EEG signals with the naked eye. In this work, we have proposed a novel computer-aided diagnosis system to detect the epilepsy using EEG signals. It is very difficult to analyze them using the conventional time-domain and frequency domain methods. Hence, we have extracted the HOS and textures features from the CWT plot. These features coupled with SVM classifier with RBF kernel yielded 96% average accuracy, average sensitivity of 96.9% and average specificity of 97% in classifying *normal*, *interictal* and *ictal* EEG signal segments. A methodology is demonstrated in this work. This accuracy is comparable with the highest accuracy reported in studies that classified all three classes. The performance of the proposed system can be further increased by using better features, more EEG data and more robust classifiers.

References

1. W. Blume, H. Lüders, E. Mizrahi, C. Tassinari, W. van Emde Boas and J. Engel, Glossary of descriptive terminology for ictal semiology: Report of the ILAE task force on classification and terminology, *Epilepsia* **42**(9) (2001) 1212–1218.
2. Commission on Epidemiology and Prognosis, International League Against Epilepsy, Guidelines for epidemiologic studies on epilepsy. Commission on Epidemiology and Prognosis, International League Against Epilepsy, *Epilepsia* **34**(4) (1993) 592–596.
3. R. Fisher, W. van Emde Boas, W. Blume, C. Elger, P. Genton, P. Lee and J. Engel, Epileptic seizures and epilepsy: Definitions proposed by the International League Against Epilepsy (ILAE) and the International Bureau for Epilepsy (IBE), *Epilepsia* **46**(4) (2005) 470–472.
4. World Health Organization, Epilepsy: Aetiogy [sic], epidemiology and prognosis, http://www.who.int/mediacentre/factsheets/fs165/en/ (accessed on March 2012).
5. D. P. Subha, K. P. Joseph, U. R. Acharya and C. M. Lim, EEG signal processing: A survey, *J. Med. Syst.* (2008), in press.
6. V. P. Nigam and D. Graupe, A neural-network-based detection of epilepsy, *Neurol. Res.* **26**(1) (2004) 55–60.
7. V. Srinivasan, C. Eswaran and N. Sriraam, Artificial neural network based epileptic detection using time-domain and frequency domain features, *J. Med. Syst.* **29**(6) (2005) 647–660.
8. H. Adeli, Z. Zhou and N. Dadmehr, Analysis of EEG records in an epileptic patient using wavelet transform, *J. Neurosc. Met.* **123**(1) (2003) 69–87.
9. H. Adeli, S. Ghosh-Dastidar and N. Dadmehr, A Wavelet-chaos methodology for analysis of EEGs and EEG sub-bands to detect seizure and epilepsy, *IEEE Trans. Biomed. Eng.* **54**(2) (2007) 205–211.
10. H. Adeli, S. Ghosh-Dastidar and N. Dadmehr, A Spatio-temporal wavelet-chaos methodology for EEG-based diagnosis of Alzheimer's diseas, *Neurosci. Lett.* **444**(2) (2008) 190–19.
11. M. Ahmadlou and H. Adeli, Wavelet synchronization methodology: A new approach for EEG-based diagnosis of ADHD, *Clinical EEG Neurosci.* **41**(1) (2010) 1–10.
12. M. Ahmadlou, H. Adeli and A. Adeli, Fractality and a wavelet-chaos-neural network methodology for EEG-based diagnosis of autistic spectrum disorder, *J. Clin. Neurophysiol.* **27**(5) (2010) 328–333.

13. A. Ahmadlou, H. Adeli and A. Adeli, Fractality and a wavelet-chao methodology for EEG-based diagnosis of Alzheime's diseas, *Alzheimer Dis. Assoc. Disord.* **25**(1) (2011) 85–92.
14. H. Adeli, S. Ghosh and Dastida, *Automated EEG Based Diagnosis of Neurological Disorders*: *Inventing the Future of Neurology* (CRC Press, 2010).
15. A. Subasi, EEG signal classification using wavelet feature extraction and a mixture of expert model, *Exp. Syst. Appl.* **32**(4) (2007) 1084–1093.
16. K. Polat and S. Guenes, Classification of epileptic form EEG using a hybrid system based on decision tree classifier and fast fourier transform, *Appl. Math. Comput.* **187**(2) (2007) 1017–1026.
17. V. Srinivasan, C. Eswaran and N. Sriraam, Approximate entropy-based epileptic EEG detection using artificial neural networks, *IEEE Trans. Inform. Technol. Biomed.* **11**(3) (2007) 288–295.
18. A. T. Tzallas, M. G. Tsipouras and D. I. Fotiadis, Automatic seizure detection based on time-frequency analysis and artificial neural networks, *Comput. Intell. Neurosci.* (2007).
19. H. Ocak, Automatic detection of epileptic seizures in EEG using discrete wavelet transform and approximate entropy, *Exp. Syst. Appl.* **36**(2) (2009) 2027–2036.
20. N. Kannathal, C. M. Lim, U. R. Acharya and P. K. Sadasivan, Entropies for detection of epilepsy in EEG, *Comput. Meth. Programs Biomed.* **80**(3) (2005) 187–194.
21. A. Subasi and M. I. Gursoy, EEG signal classification using PCA, ICA, LDA and Support Vector Machines, *Exp. Syst. Appl.* **37**(12) (2010) 8659–8666.
22. N. Kannathal, C. M. Lim, U. R. Acharya and P. K. Sadasivan, Entropies for detection of epilepsy in EEG, *Comput. Meth. Programs Biomed.* **80**(3) (2005) 187–194.
23. C. K. Chua, V. Chandran, U. R. Acharya and C. M. Lim, Automatic identification of epilepsy by HOS and power spectrum parameters using EEG signals: A comparative stud, *30th IEEE-EMBS-2008*, Vancouver, August 2008, pp. 3824–3827.
24. U. R. Acharya, E. C. P. Chua, C. K. Chua, C. M. Lim and T. Tamura, Analysis and automatic identification of sleep stages using higher order spectra, *Int. J. Neural Syst.* **20**(6) (2010) 509–521.
25. C. K. Chua, V. Chandran, U. R. Acharya and C. M. Lim, Automatic identification of epilepsy by HOS and power spectrum parameters using EEG signals: A comparative study, *29th IEEE-EMBS-2007* (2007), pp. 6495–6498.
26. EEG time series Database, http://www.meb.unibonn.de/epileptologie/science/physik/eegdata.
27. K. C. Chua, V. Chandran, U. R. Acharya and C. M. Lim, Analysis of epileptic EEG signals using higher order spectra, *J. Med. Eng. Technol.* **33**(1) (2009) 42–50.
28. U. R. Acharya, S. Vinitha, A. P. C Alvin, R. Yanti and J. S. Suri, Application of non-linear and wavelet based features for the automated identification of epileptic EEG signals, *Int. J. Neural Syst.* **22**(2) (2012) 1250002-1–1250002-14.
29. R. G. Andrzejak, K. Lehnertz, C. Rieke, F. Mormann, P. David and C. E. Elger, Indications of nonlinear deterministic and finite dimensional structures in time series of brain electrical activity: Dependence on recording region and brain state, *Phys. Rev. E* **64** (2001) 061907.
30. A. V. Medvedev, A. M. Murro and K. J. Meador, Abnormal interictal gamma activity may manifest a seizure onset zone in temporal lobe epilepsy, *Int. J. Neural Syst.* **21**(2) (2011) 103–114.
31. P. Rajdev, M. Ward and P. Irazoqui, Effect of electrical stimulation parameters on seizure treatment in the kainate animal model, *Int. J. Neural Syst.* **21**(2) (2011) 151–162.
32. S. Colici, O. C. Zalay and B. L. Bardakjian, Response neuromodulators based on artificial neural networks used to control seizure-like events in a computational model of epilepsy, *Int. J. Neural Syst.* **21**(5) (2011) 367–383.
33. S. Colici, O. C. Zalay and B. L. Bardakjian, Response neuromodulators based on artificial neural networks used to control seizure-like events in a computational model of epilepsy, *Int. J. Neural Syst.* **21**(5) (2011) 367–383.
34. S. Ghosh-Dastidar and H. Adeli, Wavelet-clustering-neural network model for freeway incident detection, *Comput.-Aided Civil Infrastruct. Eng.* **18**(5) (2003) 325–338.
35. S. Ghosh-Dastidar and H. Adeli, Neural network-wavelet micro-simulation model for delay and queue length estimation at freeway work zones, *J. Transport. Eng.* **132**(4) (2006) 331–341.
36. X. Jiang and H. Adeli, Dynamic wavelet neural network for nonlinear identification of highrise buildings, *Comput.-Aided Civil Infrastruct. Eng.* **20**(5) (2005) 316–330.
37. X. Jiang and H. Adeli, Dynamic wavelet neural network model for traffic flow forecasting, *J. Transport. Eng.* **131**(10) (2005) 771–779.
38. X. Jiang, S. Mahadevan and H. Adeli, Bayesian wavelet packet denoising for structural system identification, *Struct. Contr. Health Monit.* **14**(2) (2007) 333–356.
39. X. Jiang and H. Adeli, Pseudospectra, MUSIC, and dynamic wavelet neural network for damage detection of highrise buildings, *Int. J. Numer. Meth. Eng.* **71**(5) (2007) 606–629.
40. A. Karim and H. Adeli, Incident detection algorithm using wavelet energy representation of traffic patterns, *J. Transport. Eng.* **128**(3) (2002) 232–242.
41. A. Karim and H. Adeli, Comparison of the fuzzy — Wavelet RBFNN freeway incident detection model

with the california algorithm, *J. Transport. Eng.* **128**(1) (2002) 21–30.
42. A. Karim and H. Adeli, Fast automatic incident detection on urban and rural freeways using the wavelet energy algorithm, *J. Transport. Eng.* **129**(1) (2003) 57–68.
43. X. Jiang and H. Adeli, Dynamic fuzzy wavelet neuroemulator for nonlinear control of irregular highrise building structures, *Int. J. Numer. Meth. Eng.* **74**(7) (2008) 1045–1066.
44. H. Kim and H. Adeli, Hybrid control of smart structures using a novel wavelet-based algorithm, *Comput.-Aided Civil Infrastruct. Eng.* **20**(1) (2005) 7–22.
45. M. Vetterli, Wavelet and filter banks: Theory and design, *IEEE Trans. Signal Process.* **40**(9) (1992) 2207–2232.
46. M. Vetterli and J. Kovacevic, *Wavelets and Sub Band Coding* (Prentice-Hall, Englewood Cliffs, NJ, 1995).
47. Y. Meyer, *Wavelets and Applications* (Springer Verlag, Paris, Masson/Berlin, 1992).
48. D. A. Hein and T. Ronald, Wavelet based analysis of multi-electrode EEG-signals in epilepsy, in *Proc. SPIE*, Vol. 5839 (2005), pp. 66–74.
49. V. Chandran and S. L. Elgar, Pattern recognition using invariants defined from higher order spectra one-dimensional inputs, *IEEE Trans. Signal Process.* **41** (1997) 205–212.
50. K. C. Chua, V. Chandran, U. R. Acharya and C. M. Lim, Cardiac state diagnosis using higher order spectra of heart rate variability, *J. Med. Eng. Technol.* **32** (2006) 145–155.
51. K. C. Chua, V. Chandran, U. R. Acharya and C. M. Lim, Application of higher order spectra to identify epileptic EEG, *J. Med. Syst.* **35**(6) (2011) 1563–1571.
52. M. Mirmehdi, X. Xie and J. S. Suri, *Handbook of Texture Analysis* (Imperial College Press, 2008).
53. J. H. Tan, E. Y. K. Ng and U. R. Acharya, Study of normal ocular thermogram using textural parameters, *Infrared Phys. Technol.* **53**(2) (2010) 120–126.
54. F. Albregtsen, Statistical texture measures computed from gray level run length matrices (1995).
55. M. M. Galloway, Texture classification using gray level run length, *Comput. Graph. Image Process.* **4** (1975) 172–179.
56. T. Ojala, M. Pietikäinen and T. Maenpaa, Multiresolution gray-scale and rotation invariant texture classification with local binary patterns, *IEEE Trans. Pattern Anal. Mach. Intell.* **24** (2002) 971–987.
57. M. M. R. Krishnan, U. R. Acharya, C. Chakraborty and A. K. Ray, Automated diagnosis of oral cancer using higher order spectra features and local binary pattern: A comparative study, *Tech. Canc. Res. Treat.* **10** (2011) 433–455.
58. K. I. Laws, Rapid texture identification, *SPIE Conf. Series*, Vol. 238 (1980), pp. 376–380.
59. M. Petrou and P. G. Sevilla, *Image Processing — Dealing with Texture* (John Wiley and Sons, 2006).
60. J. Han and M. Kamber, *Data Mining*: *Concepts and Techniques*, 2nd edn. (Morgan Kaufmann, 2006).
61. J. Han, M. Kamber and J. Pei, *Data Mining*: *Concepts and Techniques* (Morgan Kaufmann, 2005).
62. S. Haykin, *Neural Networks and Learning Machines* (Prentice Hall, 2008).
63. H. Adeli and A. Panakkat, A probabilistic neural network for earthquake magnitude prediction, *Neural Netw.* **22** (2009) 1018–1024.
64. M. Ahmadlou and H. Adeli, Enhanced probabilistic neural network with local decision circles: A robust classifier, *Integr. Comput.-Aided Eng.* **17**(3) (2010) 197–210.
65. V. Vapnik, *Statistical Learning Theory* (New York, 1998).
66. C. Petitmengin, M. Baulac and V. Navarro, Seizure anticipation: Are neurophenomenological approaches able to detect pre-ictal symptoms? *Epilepsy Behav.* **9**(2) (2006) 298–306.
67. U. R. Acharya, O. Faust, N. Kannathal, T. J. Chua and S. Laxminarayan, Dinamical analysis of EEG signals at various sleep stages, *Comput. Meth. Programs Biomed.* **80**(1) (2005) 37–45.
68. J. W. Sleigh, E. Olofsen, A. Dahan, J. Goede de and A. Steyn-Ross, Entropies of the EEG: The effects of general anesthesia, in *Proc. Fifth Int. Conf. Memory, Awareness and Consciousness*, USA (2001).
69. S. Ghosh-Dastidar and H. Adeli, Improved spiking neural networks for EEG classification and epilepsy and seizure detection, *Integr. Comput.-Aided Eng.* **14**(3) (2007) 187–212.
70. S. Ghosh-Dastidar, H. Adeli and N. Dadmehr, Mixed band wavelet-chaos-neural network methodology for epilepsy and epileptic seizure detection, *IEEE Trans. Biomed. Eng.* **54**(9) (2007) 1545–1551.
71. S. Ghosh-Dastidar, H. Adeli and N. Dadmehr, Principal component analysis enhanced cosine radial basis function neural network for robust epilepsy and seizure detection, *IEEE Trans. Biomed. Eng.* **55**(2) (2008) 512–518.
72. S. Ghosh-Dastidar and H. Adeli, A new supervised learning algorithm for multiple spiking neural networks with application in epilepsy and seizure detection, *Neural Netw.* **22**(10) (2009) 1419–1431.
73. R. J. Martis, U. R. Acharya, J. H. Tan, A. Petznick, R. Yanti, C. K. Chua, E. Y. Kwee Ng and L. Tong, Application of empirical mode decomposition (EMD) for automated detection of epilepsy using EEG signals, *Int. J. Neural Syst.* (2012), in press.
74. K. C. Chua, V. Chandran, U. R. Acharya, C. M. Lim, Automatic identification of epileptic EEG signals using higher order spectra, *Int. J. Eng. Med.* **223**(4) (2009) 485–495.
75. N. F. Guler, E. D. Ubey and I. Guler, Recurrent neural network employing Lyapunov exponents for EEG

signals classification, *Exp. Syst. Appl.* **29**(3) (2005) 506–514.
76. U. R. Acharya, K. C. Chua, T. C. Lim, Dorithy and J. S. Suri, Automatic identification of epileptic EEG signals using nonlinear parameters, *J. Mech. Med. Biol.* **9**(4) (2009) 539–553.
77. U. R. Acharya, S. Vinitha, S. Chattopadhyay, W. Yu and A. P. C. Alvin, Application of recurrence quantification analysis for the automated identification of epileptic EEG signals, *Int. J. Neural Syst.* **21**(3) (2011) 199–211.
78. U. R. Acharya, F. Molinari, S. Vinitha Sree, S. Chattopadhyay, K. H. Ng and J. S. Suri, Automated diagnosis of epileptic EEG using entropies, *Biomed. Signal Process. Contr.* **7**(4) (2012) 401–408.
79. U. R. Acharya, S. Vinitha and J. S. Suri, Automatic detection of epileptic EEG signals using higher order cumulant features, *Int. J. Neural Syst.* **21**(5) (2011) 1–12.
80. O. Faust, U. R. Acharya, C. M. Lim and B. Sputh, Automatic identification of epileptic and background EEG signals using frequency domain parameters, *Int. J. Neural Syst.* **20**(2) (2010) 159–176.
81. U. R. Acharya, R. Yanti, G. Swapna, V. S. Sree, R. J. Martis and J. S. Suri, Automated diagnosis of epileptic electroencephalogram using independent component analysis and discrete wavelet transform for different electroencephalogram durations, *Proc. Inst. Mech. Eng. Pt. H J. Eng. Med.* (2012), doi: 10.1177/0954411912467883.
82. U. R. Acharya, S. Vinitha and J. S. Suri, Use of principal component analysis for automatic detection of epileptic EEG activities, *Exp. Syst. Appl.* **39**(10) (2012) 9072–9078.